



1 Investigation on the abnormal quasi-two day wave activities during
2 sudden stratospheric warming period of January 2006
3 Sheng-Yang Gu^{1,2*}, Xiankang Dou^{1,2,3}, Dora Pancheva⁴
4 ¹CAS Key Laboratory of Geospace Environment, Department of Geophysics and
5 Planetary Science, University of Science and Technology of China, Hefei, Anhui,
6 China
7 ²Mengcheng National Geophysical Observatory, School of Earth and Space Sciences,
8 University of Science and Technology of China, Hefei, Anhui, China
9 ³Wuhan University, Wuhan, China
10 ⁴National Institute of Geophysics, Geodesy and Geography, BAS, Sofia, Bulgaria
11 *Corresponding Author: Sheng-Yang Gu (gsy@ustc.edu.cn)

12
13
14



15 **Abstract**

16 The quasi-two day wave (QTDW) during austral summer period usually
17 coincides with sudden stratospheric warming (SSW) event in the winter hemisphere,
18 while the influences of SSW on QTDW are not totally understood. In this work, the
19 anomalous QTDW activities during the major SSW period of January 2006 are further
20 investigated on the basis of hourly Navy Operational Global Atmospheric Prediction
21 System-Advanced Level Physics High Altitude (NOGAPS-ALPHA) reanalysis
22 dataset. Strong westward QTDW with zonal wave number 2 (W2) is identified
23 besides the conventionally dominant mode of zonal wave number 3 (W3). Meanwhile,
24 the W3 peaks with an extremely short period of ~42 hours. Compared with January
25 2005 with no evident SSW, we found that the zonal mean zonal wind in the summer
26 mesosphere is enhanced during 2006. The enhanced summer easterly sustains critical
27 layers for W2 and short-period W3 QTDWs with larger phase speed, which facilitate
28 their amplification through wave-mean flow interaction. The stronger summer
29 easterly also provides stronger barotropic/baroclinic instabilities and thus larger
30 forcing for the amplification of QTDW. The inter-hemispheric coupling induced by
31 strong winter stratospheric planetary wave activities during SSW period is most likely
32 responsible for the enhancement of summer easterly. Besides, we found that the
33 nonlinear interaction between W3 QTDW and the wave number 1 stationary planetary
34 wave (SPW1) may also contribute to the source of W2 at middle and low latitudes in
35 the mesosphere.

36
37



38 1. Introduction

39 The temperature and wind fields in the mesopause region exhibit strong
40 oscillation with a period of several days, of which the Quasi-Two-Day wave (QTDW)
41 is the most frequently reported planetary wave (*Palo et al.*, 2007; *Limpasuvan and Wu*,
42 2009; *McCormack et al.*, 2009; *Pedatella and Forbes*, 2012; *Yue et al.*, 2012; *Chang*
43 *et al.*, 2014; *Siskind and McCormack*, 2014; *Guharay et al.*, 2015; *Lilienthal and*
44 *Jacobi*, 2015; *Madhavi et al.*, 2015; *Gu et al.*, 2016a; *Pancheva et al.*, 2016; *Wang et*
45 *al.*, 2017). There are both eastward and westward QTDWs with different zonal wave
46 numbers (*McCormack et al.*, 2014; *Gu et al.*, 2016b; *Pancheva et al.*, 2016). The
47 eastward QTDWs are usually found to exist in the winter hemisphere (*Sandford et al.*,
48 2008; *Gu et al.*, 2017), while the westward modes tend to be summer phenomena that
49 peak shortly after the solstice (*Pancheva et al.*, 2004; *Tunbridge et al.*, 2011). In the
50 southern hemisphere, the westward QTDWs show maximum amplitude during
51 January/February at middle and low latitudes (*Limpasuvan and Wu*, 2003; *Palo et al.*,
52 2007; *Gu et al.*, 2013a). In the northern hemisphere, the QTDW peaks intermittently
53 from June to August at middle latitudes (*McCormack et al.*, 2014; *Gu et al.*, 2016b;
54 *Pancheva et al.*, 2016). Generally, the QTDW activities during the austral summer
55 period are much stronger than those during boreal summer period and thus have
56 received more attention.

57 The propagation and amplification of planetary waves are intimately related to
58 the background zonal wind. As for the QTDW, it has been shown that the
59 baroclinic/barotropic instability of the summer easterly jet is an important source for
60 its amplification (*Chang et al.*, 2011; *Yue et al.*, 2012). The Eliassen-Palm (EP) flux



61 associated with QTDW grows dramatically near its critical layer (where the
62 background wind equals its phase speed), which indicates the energy transportation
63 from mean flow. The Advanced Level Physics High Altitude version of the Navy
64 Operational Global Atmospheric Prediction System (NOGAPS-ALPHA) reanalysis
65 dataset shows that the inter-annual variations of the QTDW during boreal summer
66 period are dependent on the strength of the summer easterly. A stronger summer
67 easterly provides larger forcing for its amplification (*McCormack et al.*, 2014).
68 Recently, *Gu et al.* (2016a) found that the strength of the summer easterly is also
69 responsible for the selective amplification of QTDWs with different zonal wave
70 numbers. The westward zonal wave number 2 (W2) QTDW peaks with a stronger
71 summer easterly than the westward zonal wave number 3 (W3) mode. This is because
72 a stronger summer easterly can sustain a critical layer for QTDW with larger phase
73 speed (e.g., W2), and the amplification of QTDW occurs more easily at the unstable
74 region with a critical layer (*Liu et al.*, 2004; *McCormack et al.*, 2014).

75 Sudden Stratospheric Warmings (SSWs) occur in the winter stratosphere, and are
76 most frequently observed during boreal winter period (December-February). The
77 zonal mean temperature at 10 hPa and 60°N can increase by tens of Kelvin in one or
78 two weeks during a SSW event. It is called a major SSW if the westerly wind at 10
79 hPa and 60°N reverses, while the winter westerly is slowed down but does not become
80 easterly during a minor SSW. It is generally accepted that the westward forcing from
81 the rapid amplification of planetary waves is responsible for the wind deceleration or
82 reversal in the winter stratosphere (*Matsuno*, 1971; *Liu and Roble*, 2002).



83 Interestingly, the occurrence of SSW in the northern hemisphere winter stratosphere
84 usually coincides with the temporal variation of the QTDW in the summer
85 mesosphere. Nevertheless, their influence on each other has not been totally
86 understood yet.

87 Evidence has been found for inter-hemispheric coupling during a SSW event,
88 which may have significant modulation on summer easterly jet and thus the
89 amplification of planetary waves. *Karlsson et al.* (2007) showed that the noctilucent
90 cloud in the summer mesosphere has an inverse relationship with the temperature
91 variations in the winter stratosphere. Further correlation analysis confirmed that the
92 dynamics in the winter stratosphere does have global influence on the atmospheric
93 mean state (*Karlsson et al.*, 2009; *Körnich and Becker*, 2010; *Tan et al.*, 2012). The
94 feedback between gravity-wave drag and zonal wind induced by mesospheric
95 cross-equatorial flow is a reasonable explanation for the inter-hemispheric coupling
96 mechanism. *Stray et al.* (2015) proposed that the enhancement of wave number 1 and
97 2 planetary waves at ~95 km could be a common feature during SSW period. Thus it
98 is reasonable to argue that the SSW may also have significant influence on QTDW
99 (*Lima et al.*, 2012).

100 A strong SSW event occurred in January 2006, when the QTDW activities also
101 exhibited abnormal behaviors consisting of an unusually strong W2 QTDW identified
102 in the wind and temperature fields besides the conventional W3 mode (*Varavut*
103 *Limpasuvan and Wu*, 2009). Meanwhile the W3 QTDW peaks with an extremely
104 short period of ~42 hours (*Gu et al.*, 2013a, b). It was suggested that these abnormal



105 QTDW activities may be related to the unusually strong summer easterly during the
106 same period. *McCormack et al.* (2009) proposed that the strong planetary waves
107 leading to the SSW event could influence the background zonal wind and the QTDW
108 forcing by enhancing the northward component of the residual circulation. This theory
109 was supported by simulations from the control
110 thermosphere-ionosphere-mesosphere-electrodynamics general circulation model
111 (TIME-GCM), which show that the zonal mean zonal wind and the mean flow
112 instability become stronger during a SSW event (*Gu et al.*, 2016c). Besides, they also
113 reported the nonlinear interaction between W3 QTDW and the zonal wavenumber 1
114 stationary planetary wave (SPW1), which generates a W2 QTDW (*Gu et al.*, 2015).
115 Nevertheless, unrealistic QTDW and SPW1 forcing is utilized in their numerical
116 simulation to compensate strong dissipation at lower model boundary (~10 hPa),
117 which may result in artificial nonlinear coupling. Thus, the influence of SSW on
118 QTDW needs further investigation with more realistic atmospheric conditions.

119 In addition to ground-based and satellite observations, synoptic meteorological
120 datasets could be utilized to perform diagnostic analysis on the propagation and
121 amplification of QTDW. In this paper, the anomalous QTDW activities during the
122 major SSW period of January/February 2006 will be further investigated on the basis
123 of NOGAPS-ALPHA reanalysis dataset, which has been proven to be capable of
124 reproducing both SSW and QTDW activities under realistic atmospheric conditions
125 (*McCormack et al.*, 2009). This work sheds new light on the question whether or not
126 the SSW in the winter stratosphere has significant influence on the QTDW in the



127 summer mesosphere. The dataset and analysis are briefly described in section 2. Our
128 analysis results are presented in section 3, followed by a summary in section 4.2.

129 **Datasets and analysis**

130 **2.1 Aura/MLS temperature**

131 The Aura satellite was launched on July 15, 2004, which is a major component of
132 the NASA Earth Observing System (EOS). The Microwave Limb Sounder (MLS) is
133 one of the four instruments onboard the Aura satellite that measures emissions from
134 ozone, chlorine and other trace gases with a sun-synchronous orbit (covering two
135 local times at a given latitude from ~82°S-82°N) (Schwartz et al., 2008). Aura satellite
136 travels around the earth with a period of ~99 minutes, and thus the atmosphere is
137 sampled with ~14.5 circles per day. The version 3.3 Aura/MLS temperature dataset
138 ranges from 261 hPa to 0.001 hPa (~10-96 km) with a precision of 0.6 K in the lower
139 stratosphere and 2.5 K in the mesosphere. The highest vertical resolute of 3.6 km lies
140 at 31.6 hPa, which degrades to ~6 km at 0.01 hPa. A least squares fitting method is
141 utilized to extract the QTDW information in Aura/MLS temperature from December
142 2005 to February 2006, which is then compared with the results from
143 NOGAPS-ALPHS reanalysis dataset.

144 **2.2 NOGAPS-ALPHA**

145 The NOGAPS-ALPHA reanalysis model is developed at Naval Research
146 Laboratory (NRL), which is the Advanced Level Physics High Altitude version of the
147 Navy Operational Global Atmospheric Prediction System. The NRL Atmospheric
148 Variational Data Assimilation System (NAVDAS) is adopted to incorporate both
149 ground-based and satellite observations (*Daley and Barker, 2001*), including the



150 global temperature observations from Aura/MLS and TIMED/SABER instruments.
151 The observational datasets are updated every 6 hours through the NAVDAS.
152 Nevertheless, we use the hourly meteorological fields from NOGAPS-ALPHA to
153 study the QTDWs. Please refer to *Eckermann et al.* (2009) and *Siskind et al.* (2012)
154 for more information about the model and data assimilation.

155 The NOGAPS-ALPHA reanalysis datasets have been previously used to study
156 atmospheric tides and QTDWs. For example, *Lieberman et al.* (2015) studied the
157 short-term variability of the nonmigrating tide and its relationship with the nonlinear
158 interaction between stationary planetary wave and migrating tide. *Pancheva et al.*
159 (2016) analyzed the global distribution and seasonal variation of both eastward and
160 westward propagating QTDWs. In addition, the inter-annual variability of the
161 nonlinear interactions between QTDW and migrating diurnal tide has also been
162 investigated (*McCormack et al.*, 2010; *McCormack et al.*, 2014). Their analysis
163 results show that the NOGAPS-ALPHA reanalysis model is capable of capturing tidal
164 and planetary wave behaviors in the atmosphere. We will use a two-dimensional least
165 squares fitting to extract QTDW signals in the NOGAPS-ALPHA dataset.

166 **3. Results and Discussion**

167 **3.1 QTDWs in Aura/MLS temperature**

168 Figures 1a and 1c show the spectra of the Aura/MLS temperature observation at
169 ~ 0.005 hPa during January 12-19 and 23-30 of 2006, when the W3 and W2 reach
170 maximum amplitudes (shown later by Figure 2). The MLS observations at $\sim 40^\circ\text{S}$ and
171 $\sim 20^\circ\text{S}$ are utilized in Figures 1a and 1c, respectively. It is clear that the W3 and W2
172 QTDWs dominate the wave spectra with periods of ~ 42 and ~ 45 hours, respectively.



173 The vertical and global structures of the W3 and W2 are shown in Figures 1b and 1d.
174 Most of the W3 oscillations are limited to the southern hemisphere with maximum
175 amplitude of ~12 K at ~40°N and 0.005 hPa. The temperature field of W2 exhibits
176 comparable perturbations in both hemispheres, though the branch in the southern
177 hemisphere is slightly stronger than that in the northern hemisphere. This is because
178 the larger phase speed of W2 results in more broadly distributed positive refractive
179 index, which enables its propagation in both hemispheres (*Liu et al.*, 2004; *Gu et al.*,
180 2016c). The temporal variations of the QTDWs in the summer mesosphere and the
181 zonal mean temperature in winter stratosphere are plotted in Figure 2. The W3 QTDW
182 grows as the development of SSW in early January, and reaches maximum amplitude
183 at around January 15. The W2 QTDW reaches maximum amplitude of ~6 K at around
184 January 27 with a minor peak of ~3 K at around January 10. Both the W2 and W3
185 QTDWs fade away after February 9, when the SSW also disappears and the
186 atmosphere returns to a climatological state. Figure 3 shows the comparison between
187 the QTDWs during 2005 and 2006. Abnormally strong W2 activities are observed
188 during January 2006, which are very weak during January 2005. Besides, the W3
189 QTDW is also stronger in January 2006. These QTDW activities agree well with the
190 results presented by *Limpasuvan and Wu* (2009) and *Tunbridge et al.* (2011). We will
191 then investigate whether the abnormal QTDW activities during January 2006 are
192 related to the major SSW event during the same episode with NOGAPS-ALPHA
193 reanalysis dataset.

194 3.2 QTDWs in NOGAPS-ALPHA



195 Figure 4 shows the analysis results of W2 and W3 from NOGAPS-ALPHA
196 during the same time period as Figure 1. The W3 and W2 QTDW signals are also
197 clearly indicated in the NOGAPS-ALPHA reanalysis datasets, and their vertical and
198 latitudinal temperature structures agree well with the results from Aura/MLS. Besides,
199 we found that the temporal variations of both W2 and W3 (Figure 5) are also
200 consistent with Aura/MLS observations (Figure 2). This is not strange since the
201 Aura/MLS and TIMED/SABER temperature datasets are major components
202 incorporated in the data assimilation at mesopause. We will also compare the wind
203 structures of QTDW from NOGAPS-ALPHA with those in previous literatures.
204 Figure 6 shows the zonal and meridional wind structures of W2 and W3 in
205 NOGAPS-ALPHA. The perturbations of W3 are nearly twice as strong as the W2.
206 Again, we can see that the latitudinal structures of W2 are more symmetric to the
207 equator than W3. The zonal and meridional winds of W3 peak in the southern
208 hemisphere with amplitudes of ~45 m/s and ~65 m/s at ~50°S and ~40°S, respectively.
209 The zonal wind of W2 peaks at ~20°-40° in both hemispheres with amplitudes of
210 ~10-20 m/s, while the meridional wind of W2 maximizes at the equator with
211 amplitude of ~35-40 m/s. Generally, these results agree well with previous satellite
212 observations (*Limpasuvan and Wu, 2009; Gu et al., 2013a*). Thus we conclude that
213 both the temperature and wind fields in NOGAPS-ALPHA are reasonable and
214 comparable with realistic atmospheric state, which can be utilized in the mechanical
215 study of the anomalous QTDW activities during January 2006.

216 It is proposed that the SSW may have significant influence on QTDW by



217 changing the mean flow (*Gu et al.*, 2016c). Thus we will first show how the
 218 background wind influences the amplification of QTDWs. A necessary condition for
 219 the occurrence of baroclinic/barotropic instability for zonal mean zonal wind is $\bar{q}_\varphi < 0$,
 220 where \bar{q}_φ is the latitudinal gradient of the quasi-geostrophic potential vorticity (*Liu et*
 221 *al.*, 2004):

$$222 \quad \bar{q}_\varphi = 2\Omega \cos \varphi - \left(\frac{\bar{u} \cos \varphi}{a \cos \varphi} \right)_\varphi - \frac{a}{\rho} \left(\frac{f^2}{N^2} \rho \bar{u}_z \right)_z \quad (1)$$

223 where \bar{u} , a , φ , f , N , Ω , and ρ are the zonal mean zonal wind, earth radius, latitude,
 224 Coriolis parameter, Brunt-Väisällä frequency, angular speed of the earth's rotation,
 225 and the background air density, z means the vertical gradient. Planetary waves can be
 226 amplified by the instabilities through mean-flow interaction. It has been found that the
 227 EP flux of QTDW grows dramatically after the over-reflection by its critical layer
 228 near the unstable region (*Liu et al.*, 2004). The EP flux of planetary waves, (e.g.,
 229 QTDW), can be calculated following *McCormack et al.* (2014):

$$230 \quad \vec{F}_{EP} = \rho a \cos \varphi \begin{bmatrix} -\overline{v' u'} \\ \left[f - \frac{(\bar{u} \cos \varphi)_\varphi}{a \cos \varphi} \right] \overline{v' \theta'} \\ \overline{\theta'_z} \end{bmatrix} \quad (2)$$

231 where u' , v' , and θ' are the zonal wind, meridional wind, and potential temperature
 232 perturbations of planetary waves.

233 The barotropic/baroclinic instabilities of the mean flow and the EP flux of W2
 234 and W3 are shown in Figure 7. It is clear that the W3 is more favorable to propagate
 235 in the summer hemisphere, and is dramatically amplified by the mean flow
 236 instabilities at middle latitude between 0.1 and 0.01 hPa. Nevertheless, the W2 is



237 capable of propagating in both hemispheres due to its broadly distributed refractive
238 index (*Gu et al.*, 2016c). The summer branch is also amplified by the instabilities
239 related to the easterly wind, while the winter branch propagates directly from the
240 lower atmosphere to mesosphere. *Liu et al.* (2004) has shown that the amplification of
241 QTDW through wave-mean flow interaction most easily occurs near its critical layer,
242 which is also indicated in our analysis.

243 Figure 2 has shown that both the QTDWs and the SSW peak in the middle and
244 late January, thus Figure 8 shows the comparison between the zonal mean zonal wind
245 during January 11-30 of 2005 and 2006. The zonal wind during the SSW period of
246 2006 shows two major differences compared with that in 2005. First, the westerly
247 wind in winter stratosphere reverses to easterly. The winter westerly reversal is one
248 key feature of major SSW, which is induced by the rapid growth of stationary
249 planetary waves and their momentum deposition to the background mean flow (*Liu*
250 *and Roble*, 2002). Second, the summer easterly wind in the mesosphere is enhanced.
251 The interhemispheric couplings during SSW period have been reported in previous
252 literatures (*Karlsson et al.*, 2007, 2009; *Körnich and Becker*, 2010). We then analyzed
253 the correlation between the temporal variations of the global zonal mean zonal wind
254 and the zonal mean temperature at 70°N and 10 hPa, which increase dramatically
255 during a SSW event. The correlation coefficients are shown in Figure 9. The zonal
256 wind in the summer mesosphere at middle latitude shows a significant inverse
257 relationship with the temperature variations in the winter stratosphere. In the summer
258 hemisphere, the zonal mean zonal wind is westward in the upper stratosphere and



259 mesosphere; it will be enhanced when the temperature in winter stratosphere increases.
260 Thus, we conclude that the zonal wind anomaly during January 2006 is most likely
261 correlated with the SSW event.

262 We then show how these differences result in different QTDW behaviors during
263 2005 and 2006. The mean flow instabilities of the background wind and the critical
264 layers of W2 and W3 are shown in Figure 10. First the enhanced summer easterly in
265 the mesosphere results in stronger barotropic/baroclinic instability, which provides
266 larger forcing for the amplification of QTDW. This results in stronger W3 amplitude
267 during 2006 than that during 2005 (Figure 3). Besides, the stronger summer easterly
268 in the mesosphere also sustains a critical layer for W2 during 2006 at middle latitude,
269 which is not observed in 2005. The phase speed of planetary wave is inversely
270 proportional to both period and zonal wave numbers, thus the phase speed of W2 is
271 larger than W3. The existence of W2 critical layer nearby the instability region
272 facilitates the wave-mean flow interaction, through which the energy of mean flow is
273 transferred to W2 (*Liu et al.*, 2004). This results in abnormally strong W2 oscillations
274 in 2006 than that in 2005. *Gu et al.* (2013b) also noted that the W3 during 2006 peaks
275 with an extremely short period of ~42 hours (also shown by Figure 1 and 4), whereas
276 the period of W3 during austral summer tends to be longer (~52 hours) (*Palo et al.*,
277 2007; *Tunbridge et al.*, 2011; *Yue et al.*, 2012). The W3 QTDW with a longer period
278 has a slower phase speed. Figure 11 shows the comparison between the critical layers
279 of 42- and 52-hour W3 for the zonal mean state during 2006. The critical layer of the
280 42-hour W3 runs at the edge of the mean flow instability, which is totally surrounded



281 by the critical layer of the 52-hour W3. Thus the 52-hour QTDW signal has already
282 been reflected away by the critical layer before it reaches the unstable region and
283 cannot be amplified through wave-mean flow interaction (*Liu et al.*, 2004). Figure
284 10b also shows that both the critical layers of W3 and W2 run across the mean flow
285 instabilities in winter stratospheric region, whereas there is no significant positive EP
286 flux divergence near this region (Figure 12) as that shown in the summer mesosphere.
287 Positive EP flux divergence indicates the source for planetary waves. Thus we
288 conclude that the mean flow instability related to the winter westerly reversal during
289 SSW period is not as effective for the QTDW amplification as that in the summer
290 mesosphere.

291 **3.3 The nonlinear coupling between W3 and SPW1**

292 *Gu et al.* (2015) proposed that the nonlinear interaction between W3 and SPW1
293 could also provide sources for W2. We also calculated the nonlinear advection
294 between W3 and SPW1 following *Gu et al.* (2016c), which is shown Figure 13. The
295 nonlinear advection from TIME-GCM shows a significant peak at the lower boundary
296 (~10 hPa) in the winter stratosphere (Figure 13 of *Gu et al.* (2016c)), which is not
297 shown by our results from NOGAPS-ALPHA. Note that both the W3 and SPW1 is
298 forced at the lower model boundary in TIME-GCM (~10 hPa), which is much
299 stronger than realistic situation to compensate the large dissipation. Thus we conclude
300 that the nonlinear advection between W3 and SPW1 is in fact insignificant in the
301 winter stratosphere. Besides, the nonlinear advection also shows four peaks in the
302 mesosphere. The peak in polar winter mesosphere (~85°N, 0.01 hPa) is most possibly



303 related to the strong wave number 1 component of the wind oscillations, which is
304 shown by Figure 14. Considering that the W2 is only favored to propagate at middle
305 and low latitudes (*Gu et al.*, 2016c), the nonlinear coupling between W3 and SPW1 in
306 the winter polar region maybe ineffective for the observed W2 perturbations. There
307 are both significant wind perturbations for W3 and SPW1 at low latitudes in the
308 northern hemisphere (Figure 14), and their nonlinear advection reaches ~12-15
309 m/s/day in this region. This agrees well with the result from TIME-GCM and possibly
310 contributes to the northern branch of W2 (Figure 7b). The EP flux divergence of W2
311 in Figure 12 also shows a source at ~10°N between 0.01 and 0.001 hPa, which is
312 possibly related to the nonlinear advection between W3 and SPW1. The wind
313 perturbations of W3 reach maximum amplitude at middle and low latitudes in the
314 summer mesosphere, and the nonlinear advection also reaches ~15 m/s/day and ~9
315 m/s/day at ~50°S and ~10°S, respectively. These nonlinear couplings may contribute
316 to the southern branch of W2 (Figure 7b) and its positive EP flux divergence at ~25°S
317 between 0.01 and 0.001 hPa (Figure 12a).

318 Though the W3 and SPW1 shows significant nonlinear coupling at middle and
319 low latitudes in the mesosphere, this does not mean that the nonlinear interaction is
320 the only source for W2. The EP flux of W2 in the winter stratosphere shows clear
321 upward propagation tendency, which most probably originates from the lower
322 atmosphere (Figure 15). The strong planetary wave activity in winter hemisphere,
323 which is responsible for the occurrence of SSW, may also provide strong sources for
324 QTDW in the lower atmosphere. *Gu et al.* (2016a, b) also showed that there are



325 persistent QTDW signals in the lower atmosphere, whereas the amplification of
326 QTDW in the mesosphere is dependent on the strength of the summer easterly. The
327 interhemispheric coupling during SSW period results in strong summer easterly jet in
328 January 2006, which provides suitable condition for the amplification of W2 signals
329 in the lower hemisphere.

330 **4. Summary**

331 In this paper, the influence of SSW on QTDWs is further investigated with
332 NOGAPS-ALPHA reanalysis dataset, which is a further contribution to previous work
333 reported by *Gu et al.* (2016c). Their TIME-GCM simulations use a climatological
334 atmosphere state as the background and the planetary waves are forced at the lower
335 model boundary (~10 hPa), which may induce artificial signals. Nevertheless, the
336 NOGAPS-ALPHA reanalysis dataset incorporates realistic observation from the
337 ground to mesosphere, which avoids the lower boundary effect. Our analysis shows
338 that the nonlinear interaction between W3 and SPW1 most probably occurs at middle
339 and low latitudes in the mesosphere.

340 During the major SSW period of January 2006, the QTDWs exhibit strong
341 oscillations with zonal wave number 2 and the conventional wave number 3 mode
342 peaks at an extremely short period. We found that the inter-hemispheric coupling
343 induced by strong winter planetary wave activities plays a crucial role in connecting
344 the winter stratospheric SSW and the summer mesospheric QTDW. To be exact, the
345 summer easterly is enhanced during a SSW event through the inter-hemispheric
346 coupling, which results in anomalous QTDW behaviors. The enhanced summer
347 easterly can sustain critical layers for QTDW with larger phase speed (e.g., smaller



348 zonal wave number, short period), which facilitate their amplification through
349 wave-mean flow interactions. Moreover, the enhanced summer easterly also provides
350 stronger barotropic/baroclinic instabilities and thus a larger forcing for the
351 amplification of QTDW, which results in strong W3 oscillation during January 2006.
352 Thus, we conclude that the abnormal QTDW activities in the summer mesosphere
353 observed by *Limpasuvan and Wu* (2009) are correlated with the major SSW event in
354 the winter stratosphere through inter-hemispheric coupling. We should note that the
355 summer easterly may also exhibits strong inter-annual variations, which could result
356 in different QTDW activities during other SSW years. A detailed comparison between
357 the QTDWs (with different zonal wave numbers) during SSW and non-SSW years
358 will be statistically studied in the future.

359 **Acknowledgement**

360 This work is sponsored by the Project Funded by China Postdoctoral Science
361 Foundation (2015M582001, 2016T90573), the National Natural Science Foundation
362 of China (41421063, 41304123), and Hundred Talents Program (D). The
363 NOGAPS-ALPHA dataset is available at <ftp://map.nrl.navy.mil/pub/nrl/nogaps> and the
364 Aura/MLS temperature observation can be downloaded by
365 <https://disc.sci.gsfc.nasa.gov/Aura/data-holdings/MLS>.

366



367 **References**

- 368 Chang, L. C., S. E. Palo, and H. L. Liu (2011), Short-term variability in the migrating
369 diurnal tide caused by interactions with the quasi 2 day wave, *Journal of*
370 *Geophysical Research-Atmospheres*, *116*.
- 371 Chang, L. C., J. Yue, W. Wang, Q. Wu, and R. R. Meier (2014), Quasi two day
372 wave-related variability in the background dynamics and composition of the
373 mesosphere/thermosphere and the ionosphere, *Journal of Geophysical Research:*
374 *Space Physics*, *119*(6), 4786-4804.
- 375 Daley, R., and E. Barker (2001), NAVDAS: Formulation and diagnostics, *Mon*
376 *Weather Rev*, *129*(4), 869-883.
- 377 Eckermann, S. D., et al. (2009), High-altitude data assimilation system experiments
378 for the northern summer mesosphere season of 2007, *Journal of Atmospheric*
379 *and Solar-Terrestrial Physics*, *71*(3-4), 531-551.
- 380 Gu, S.-Y., H.-L. Liu, N. M. Pedatella, X. Dou, and Z. Shu (2016a), The quasi-2day
381 wave activities during 2007 boreal summer period as revealed by Whole
382 Atmosphere Community Climate Model, *Journal of Geophysical Research:*
383 *Space Physics*, *121*(7), 7256-7268.
- 384 Gu, S.-Y., H.-L. Liu, N. M. Pedatella, X. Dou, T. Li, and T. Chen (2016b), The quasi 2
385 day wave activities during 2007 austral summer period as revealed by Whole
386 Atmosphere Community Climate Model, *Journal of Geophysical Research:*
387 *Space Physics*, *121*(3), 2743-2754.
- 388 Gu, S.-Y., H.-L. Liu, N. M. Pedatella, X. Dou, and Y. Liu (2017), On the wave
389 number 2 eastward propagating quasi 2 day wave at middle and high latitudes, J.



- 390 Geophys. Res. Space Physics, 122, 4489–4499, doi:10.1002/2016JA023353.
- 391 Gu, S.-Y., H.-L. Liu, T. Li, X. Dou, Q. Wu, and J. M. Russell (2015), Evidence of
392 nonlinear interaction between quasi 2 day wave and quasi-stationary wave,
393 *Journal of Geophysical Research: Space Physics*, 120(2), 1256-1263.
- 394 Gu, S. Y., H. L. Liu, X. Dou, and T. Li (2016c), Influence of the sudden stratospheric
395 warming on quasi-2-day waves, *Atmos. Chem. Phys.*, 16(8), 4885-4896.
- 396 Gu, S. Y., T. Li, X. K. Dou, Q. Wu, M. G. Mlynczak, and J. M. Russell (2013a),
397 Observations of Quasi-Two-Day wave by TIMED/SABER and TIMED/TIDI,
398 *Journal of Geophysical Research-Atmospheres*, 118(4), 1624-1639.
- 399 Gu, S. Y., T. Li, X. Dou, N.-N. Wang, D. Riggin, and D. Fritts (2013b), Long-term
400 observations of the quasi two-day wave by Hawaii MF radar, *Journal of*
401 *Geophysical Research: Space Physics*, 118(12), 2013JA018858.
- 402 Guharay, A., P. P. Batista, and B. R. Clemesha (2015), Variability of the quasi-2-day
403 wave and interaction with longer period planetary waves in the MLT at
404 Cachoeira Paulista (22.7°S, 45°W), *Journal of Atmospheric and Solar-Terrestrial*
405 *Physics*, 130–131, 57-67.
- 406 Körnich, H., and E. Becker (2010), A simple model for the interhemispheric coupling
407 of the middle atmosphere circulation, *Advances in Space Research*, 45(5),
408 661-668.
- 409 Karlsson, B., H. Körnich, and J. Gumbel (2007), Evidence for interhemispheric
410 stratosphere-mesosphere coupling derived from noctilucent cloud properties,
411 *Geophysical Research Letters*, 34(16), L16806.



- 412 Karlsson, B., C. McLandress, and T. G. Shepherd (2009), Inter-hemispheric
413 mesospheric coupling in a comprehensive middle atmosphere model, *Journal of*
414 *Atmospheric and Solar-Terrestrial Physics*, 71(3–4), 518-530.
- 415 Lieberman, R. S., D. M. Riggin, D. A. Ortland, J. Oberheide, and D. E. Siskind (2015),
416 Global observations and modeling of nonmigrating diurnal tides generated by
417 tide-planetary wave interactions, *Journal of Geophysical Research: Atmospheres*,
418 120(22), 11,419-411,437.
- 419 Lilienthal, F., and C. Jacobi (2015), Meteor radar quasi 2-day wave observations over
420 10 years at Collm (51.3° N, 13.0° E), *Atmos. Chem. Phys.*, 15(17), 9917-9927.
- 421 Lima, L. M., E. O. Alves, P. P. Batista, B. R. Clemesha, A. F. Medeiros, and R. A.
422 Buriti (2012), Sudden stratospheric warming effects on the mesospheric tides
423 and 2-day wave dynamics at 7°S, *J. Atmos. Sol. Terr. Phys.*, 78–79, 99–107,
424 doi:10.1016/j.jastp.2011.02.013.
- 425 Limpasuvan, V., and D. L. Wu (2003), Two-day wave observations of UARS
426 Microwave Limb Sounder mesospheric water vapor and temperature, *Journal of*
427 *Geophysical Research-Atmospheres*, 108(D10), -.
- 428 Limpasuvan, V., and D. L. Wu (2009), Anomalous two-day wave behavior during the
429 2006 austral summer, *Geophys. Res. Lett.*, 36(4), L04807.
- 430 Liu, H. L., and R. G. Roble (2002), A study of a self-generated stratospheric sudden
431 warming and its mesospheric-lower thermospheric impacts using the coupled
432 TIME-GCM/CCM3, *J. Geophys. Res.*, 107(D23), 4695.
- 433 Liu, H. L., E. R. Talaat, R. G. Roble, R. S. Lieberman, D. M. Riggin, and J. H. Yee



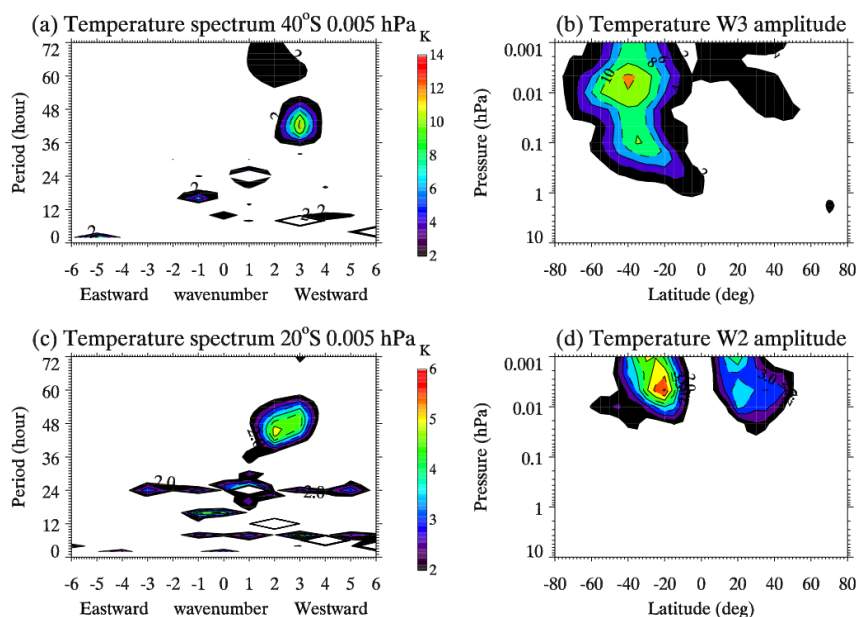
- 434 (2004), The 6.5-day wave and its seasonal variability in the middle and upper
435 atmosphere, *J. Geophys. Res.*, *109*(D21), D21112.
- 436 Madhavi, G. N., P. Kishore, S. V. B. Rao, I. Velicogna, and G. Basha (2015), Two-day
437 wave observations over the middle and high latitudes in the NH and SH using
438 COSMIC GPSRO measurements, *Advances in Space Research*, *55*(2), 722-731.
- 439 Matsuno, T. (1971), A Dynamical Model of the Stratospheric Sudden Warming,
440 *Journal of the Atmospheric Sciences*, *28*(8), 1479-1494.
- 441 McCormack, J. P., L. Coy, and K. W. Hoppel (2009), Evolution of the quasi 2-day
442 wave during January 2006, *J. Geophys. Res.*, *114*(D20), D20115.
- 443 McCormack, J. P., L. Coy, and W. Singer (2014), Intraseasonal and interannual
444 variability of the quasi 2 day wave in the Northern Hemisphere summer
445 mesosphere, *Journal of Geophysical Research: Atmospheres*, *119*(6), 2928-2946.
- 446 McCormack, J. P., S. D. Eckermann, K. W. Hoppel, and R. A. Vincent (2010),
447 Amplification of the quasi-two day wave through nonlinear interaction with the
448 migrating diurnal tide, *Geophys. Res. Lett.*, *37*(16), L16810.
- 449 Palo, S. E., J. M. Forbes, X. Zhang, J. M. Russell III, and M. G. Mlynczak (2007), An
450 eastward propagating two-day wave: Evidence for nonlinear planetary wave
451 and tidal coupling in the mesosphere and lower thermosphere, *Geophys. Res.*
452 *Lett.*, *34*, L07807, doi:10.1029/2006GL027728.
- 453 Pancheva, D., P. Mukhtarov, D. E. Siskind, and A. K. Smith (2016), Global
454 distribution and variability of quasi 2 day waves based on the NOGAPS-ALPHA
455 reanalysis model, *Journal of Geophysical Research: Space Physics*, n/a-n/a.



- 456 Pancheva, D. M., N. J.; Manson, A. H.; Meek, C. E.; Jacobi, Ch.; Portnyagin, Yu.;
457 Merzlyakov, E.; Hocking, W. K.; MacDougall, J.; Singer, W.; Igarashi, K.; Clark,
458 R. R.; Riggin, D. M.; Franke, S. J.; Kürschner, D.; Fahrutdinova, A. N.; Stepanov,
459 A. M.; Kashcheyev, B. L.; Oleynikov, A. N.; Muller, H. G. (2004), Variability of
460 the quasi-2-day wave observed in the MLT region during the PSMOS campaign
461 of June-August 1999, *Journal of Atmospheric and Solar-Terrestrial Physics*,
462 66(6-9), 539-565.
- 463 Pedatella, N. M., and J. M. Forbes (2012), The quasi 2 day wave and spatial-temporal
464 variability of the OH emission and ionosphere, *J. Geophys. Res.*, 117(A1),
465 A01320.
- 466 Sandford, D. J., M. J. Schwartz, and N. J. Mitchell (2008), The wintertime two-day
467 wave in the polar stratosphere, mesosphere and lower thermosphere, *Atmos.*
468 *Chem. Phys.*, 8(3), 749–755, doi:10.5194/acp-8-749-2008.
- 469 Schwartz, M.J., Lambert, A., Manney, G.L., et al., 2008. Validation of the Aura
470 microwave limb sounder temperature and geopotential height measurements. *J.*
471 *Geophys. Res.* 113, D15S11. <http://dx.doi.org/10.1029/2007JD008783>.
- 472 Siskind, D. E., and J. P. McCormack (2014), Summer mesospheric warmings and the
473 quasi 2 day wave, *Geophysical Research Letters*, 2013GL058875.
- 474 Siskind, D. E., D. P. Drob, J. T. Emmert, M. H. Stevens, P. E. Sheese, E. J. Llewellyn,
475 M. E. Hervig, R. Niciejewski, and A. J. Kochenash (2012), Linkages between the
476 cold summer mesopause and thermospheric zonal mean circulation, *Geophysical*
477 *Research Letters*, 39(1).



- 478 Stray, N. H., Y. J. Orsolini, P. J. Espy, V. Limpasuvan, and R. E. Hibbins (2015),
479 Observations of planetary waves in the mesosphere-lower thermosphere during
480 stratospheric warming events, *Atmos. Chem. Phys.*, 15(9), 4997-5005.
- 481 Tan, B., X. Chu, H.-L. Liu, C. Yamashita, and J. M. Russell, III (2012), Zonal-mean
482 global teleconnection from 15 to 110 km derived from SABER and WACCM, *J.*
483 *Geophys. Res.*, 117(D10), D10106.
- 484 Tunbridge, V. M., D. J. Sandford, and N. J. Mitchell (2011), Zonal wave numbers of
485 the summertime 2 day planetary wave observed in the mesosphere by EOS Aura
486 Microwave Limb Sounder, *J. Geophys. Res.*, 116(D11), D11103.
- 487 Wang, J. C., L. C. Chang, J. Yue, W. Wang, and D. E. Siskind (2017), The quasi 2 day
488 wave response in TIME-GCM nudged with NOGAPS-ALPHA, *Journal of*
489 *Geophysical Research: Space Physics*, 122, doi:10.1002/2016JA023745.
- 490 Yue, J., H.-L. Liu, and L. C. Chang (2012), Numerical investigation of the quasi 2 day
491 wave in the mesosphere and lower thermosphere, *J. Geophys. Res.*, 117(D5),
492 D05111.
493



494

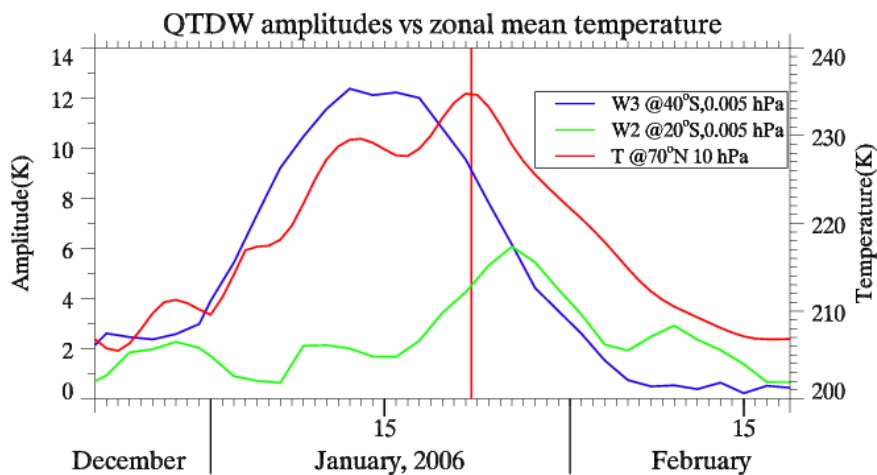
495 Figure 1 The wave number-period spectra of the Aura/MLS temperature observations
496 during (a) January 12-19 of 2006 at $\sim 40^{\circ}\text{S}$ and ~ 0.005 hPa, (c) January 23-30 of 2006
497 at $\sim 20^{\circ}\text{S}$ and ~ 0.005 hPa. The corresponding latitudinal and vertical structures of the
498 W3 and W2 QTDWs are shown in (b) and (d), respectively.

499

500



501



502

503

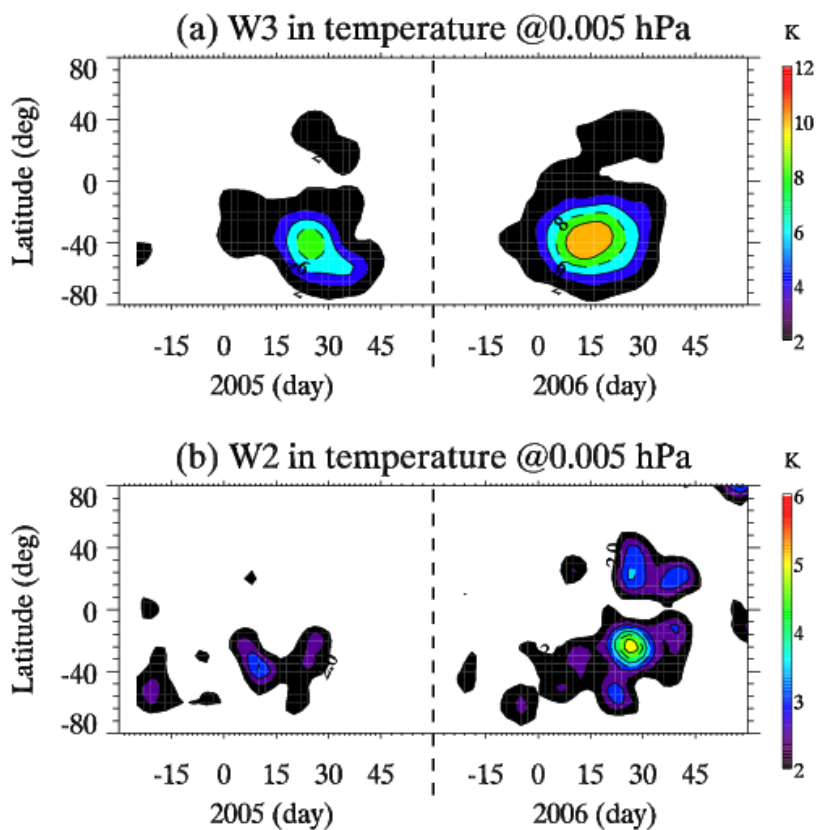
504

505

506

507

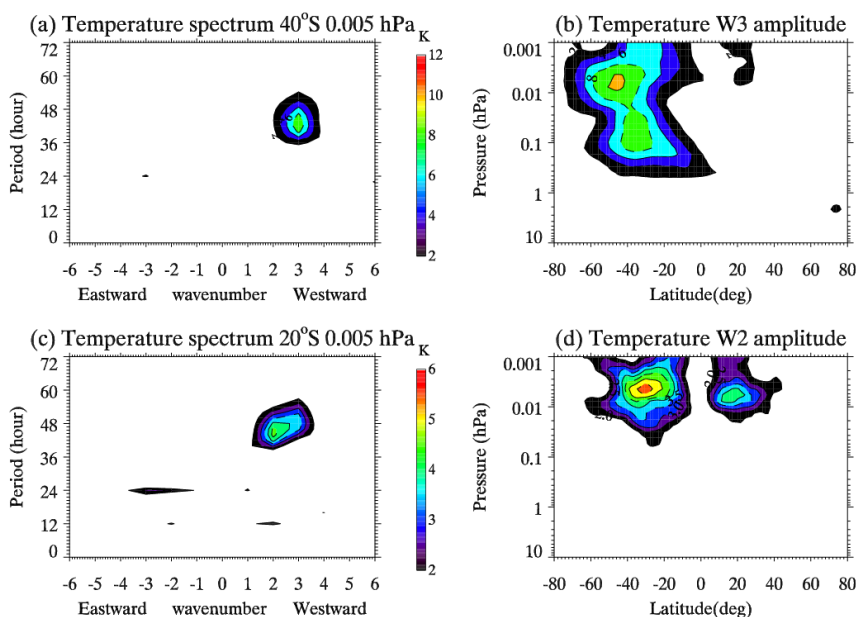
Figure 2 The temporal variations of the (blue) W3 at $\sim 40^{\circ}\text{S}$ and (green) W2 at $\sim 20^{\circ}\text{S}$. The zonal mean temperature at 70°N and 10 hPa is also plotted (red). The Aura/MLS temperature observations are utilized in the analysis. The vertical red line indicates the warming peak of the SSW.



508

509 Figure 3 Temporal variations of the (a) W3 and (b) W2 in Aura/MLS temperature
510 observations at ~0.005 hPa during 2005 and 2006.

511

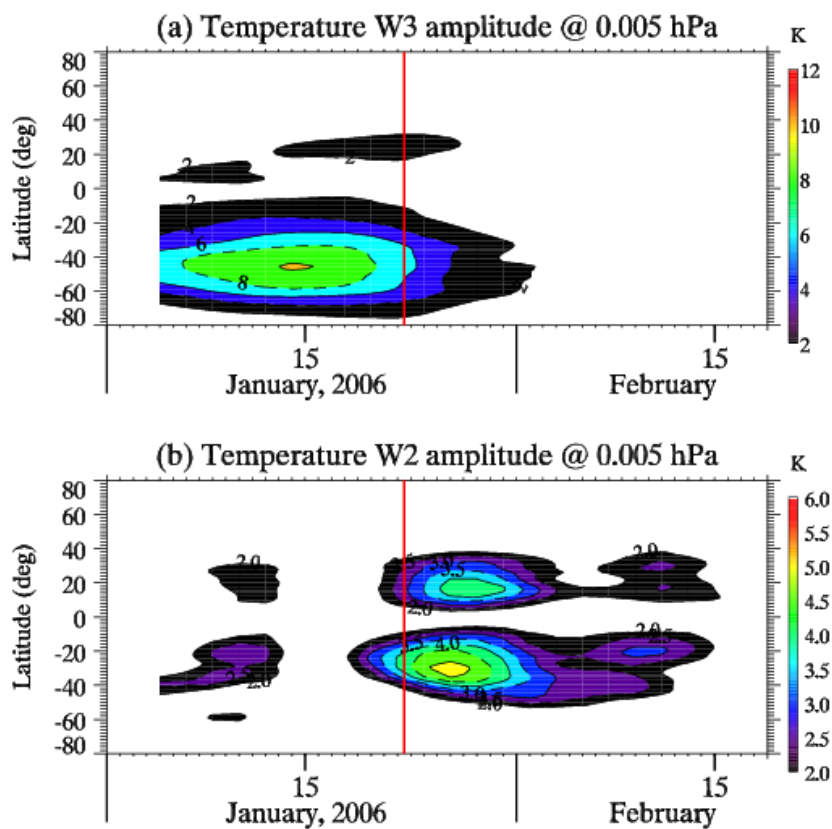


512
513
514

Figure 4 The same as Figure 1 but for the NOGAPS-ALPHA reanalysis datasets.



515



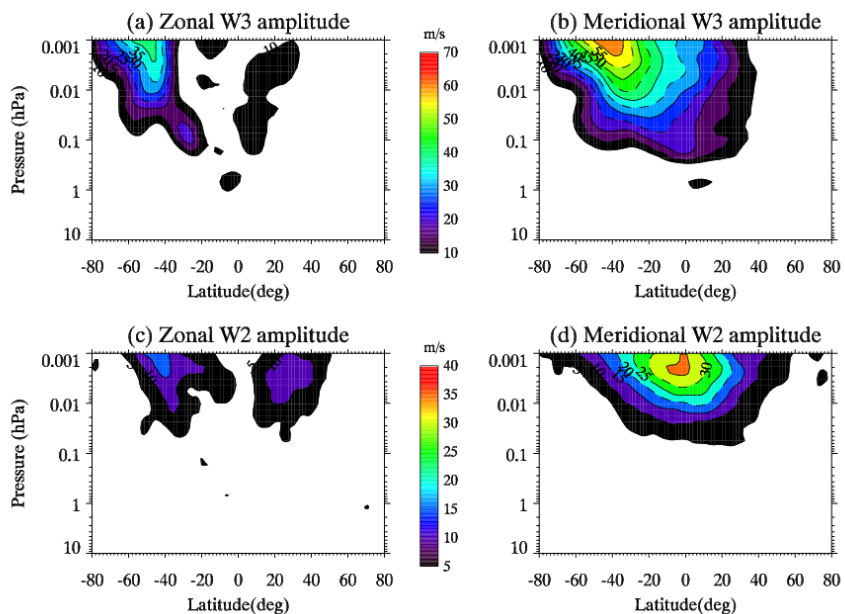
516

517 Figure 5 Temporal variations of the (a) W3 and (b) W2 QTDWs at ~0.005 hPa during
518 2006 from NOGAPS-ALPHA reanalysis dataset. The vertical red lines indicate the
519 warming peak of SSW.

520



521



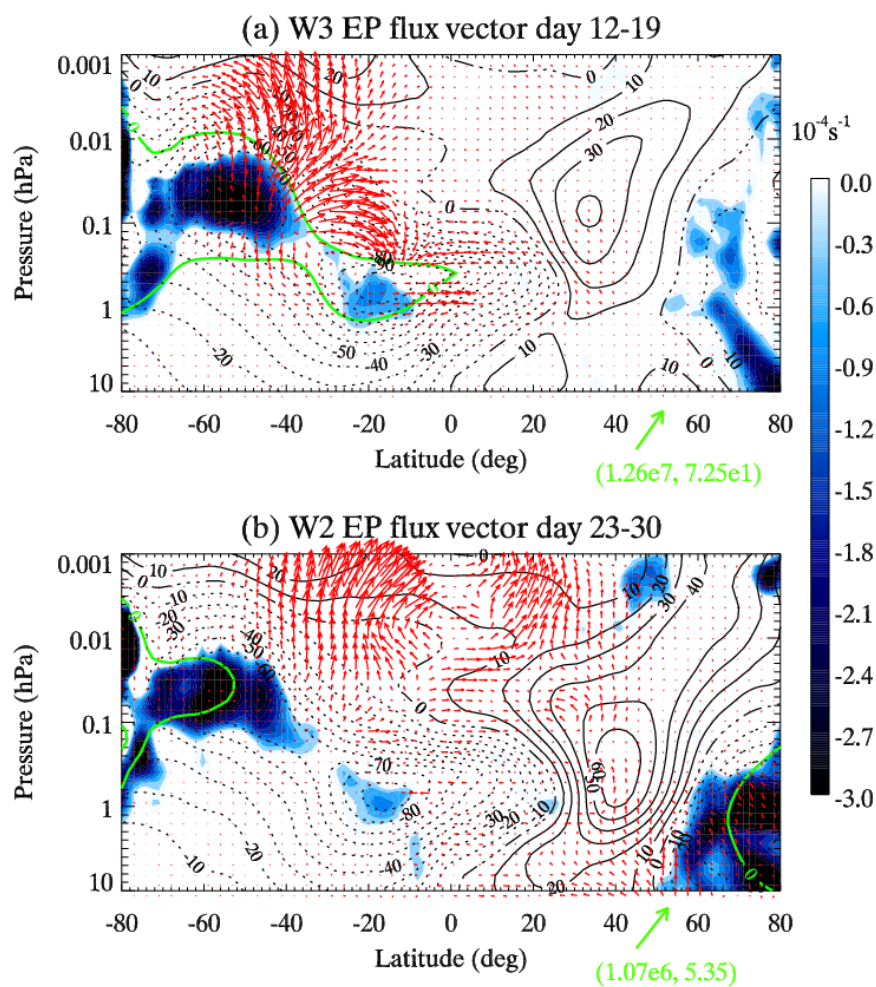
522

523 Figure 6 Altitude-latitude structures of the (a, b) W3 and (b, d) W2 in (a, c) zonal and
524 (b, d) meridional wind components. The wind fields during January 12-19 and 23-30
525 of 2006 are utilized for the analysis of W3 and W2, respectively.

526



527



528

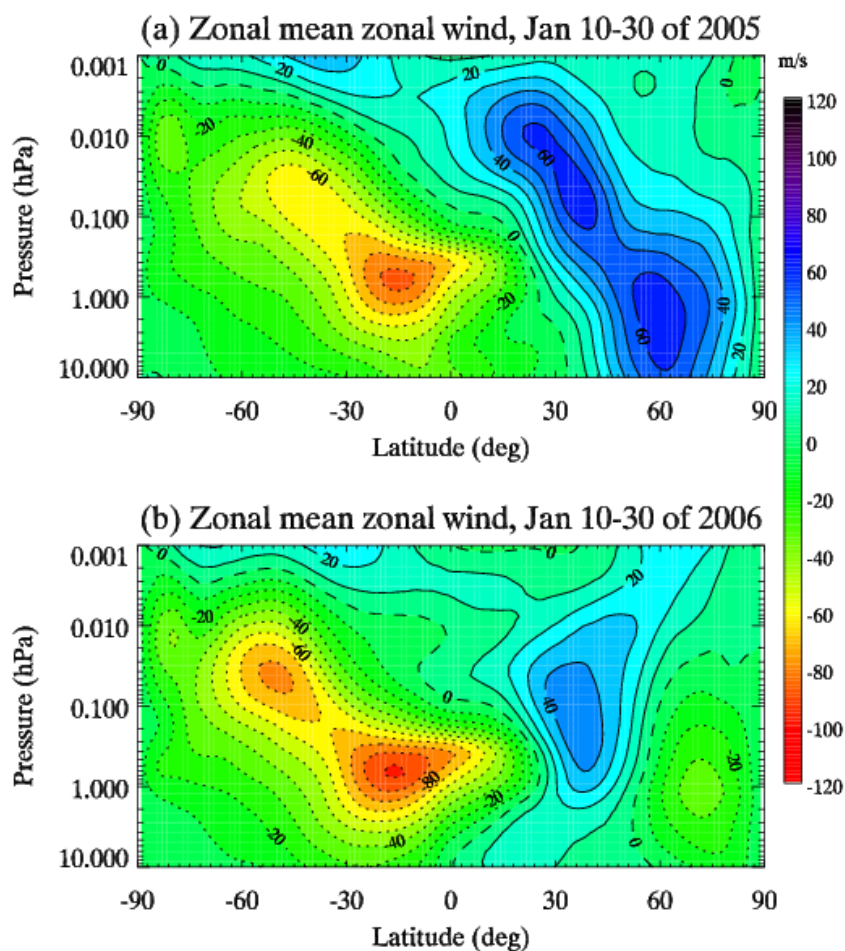
529 Figure 7 The EP flux vectors of (a) W3 during January 12-19 and (b) W2 during

530 January 23-30. The barotropically/baroclinically unstable regions ($\bar{q}_\phi < 0$, equation 1)

531 are shaded with blue, and the critical layers are overplotted with green lines. The EP

532 flux vectors are normalized by the square root of the neutral density. The reference

533 lengths are shown at right bottom.

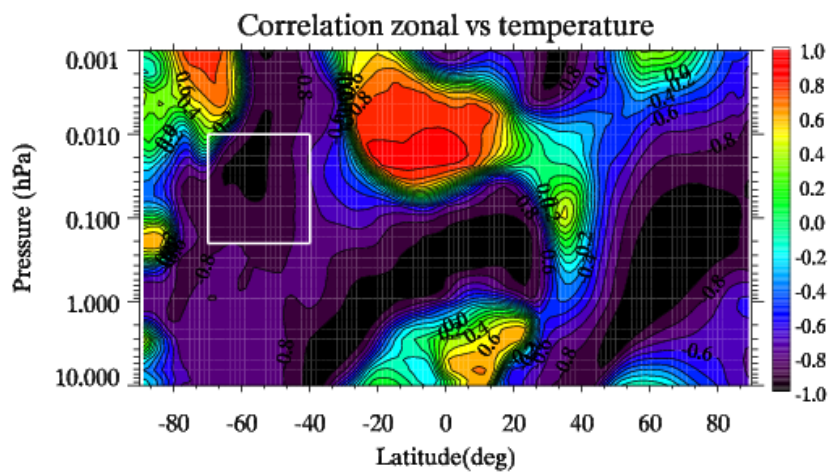


534

535 Figure 8 The zonal mean zonal wind during days 10-30 of (a) 2005 and (b) 2006. The

536 eastward and westward winds are plotted with solid and dotted lines, respectively.

537



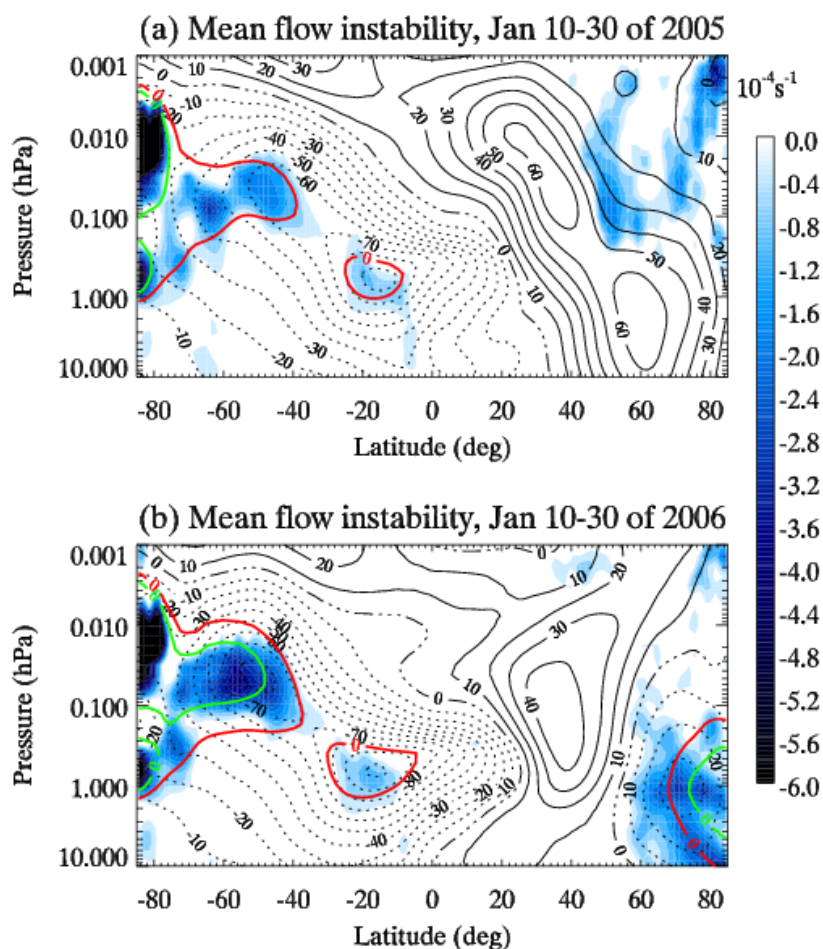
538

539 Figure 9 The correlation coefficient between the global zonal mean zonal wind and
540 the temperature at 10 hPa and 70°N from January 1 to February 20 of 2006. The
541 rectangle indicates the unstable region that contributes most significantly to the
542 amplification of QTDW.

543



544



545

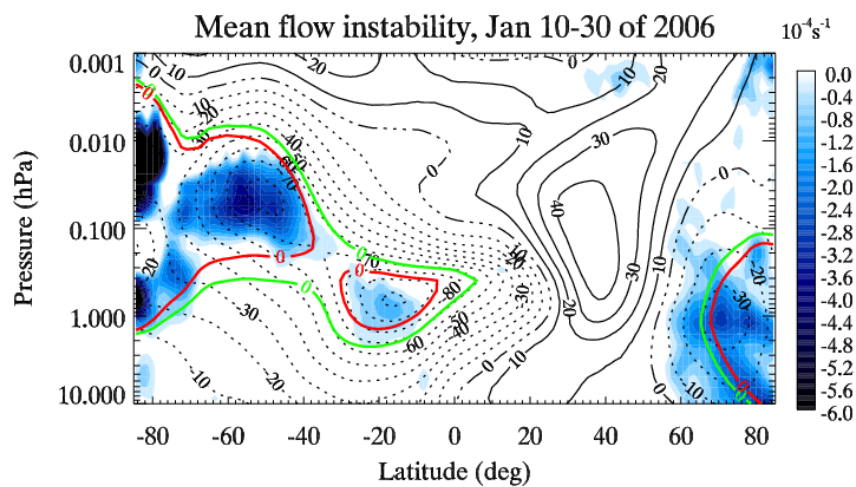
546 Figure 10 Comparison between the critical lines of the (red) 42-hour W3 and (light
547 green) 45-hour W2 for zonal mean zonal wind during days 10-30 of (a) 2005 and (b)
548 2006. The westward (eastward) zonal wind is plotted with dot (solid) lines, and the

549 barotropically/baroclinically unstable regions ($\bar{q}_\phi < 0$, equation 1) are shaded with
550 blue.

551



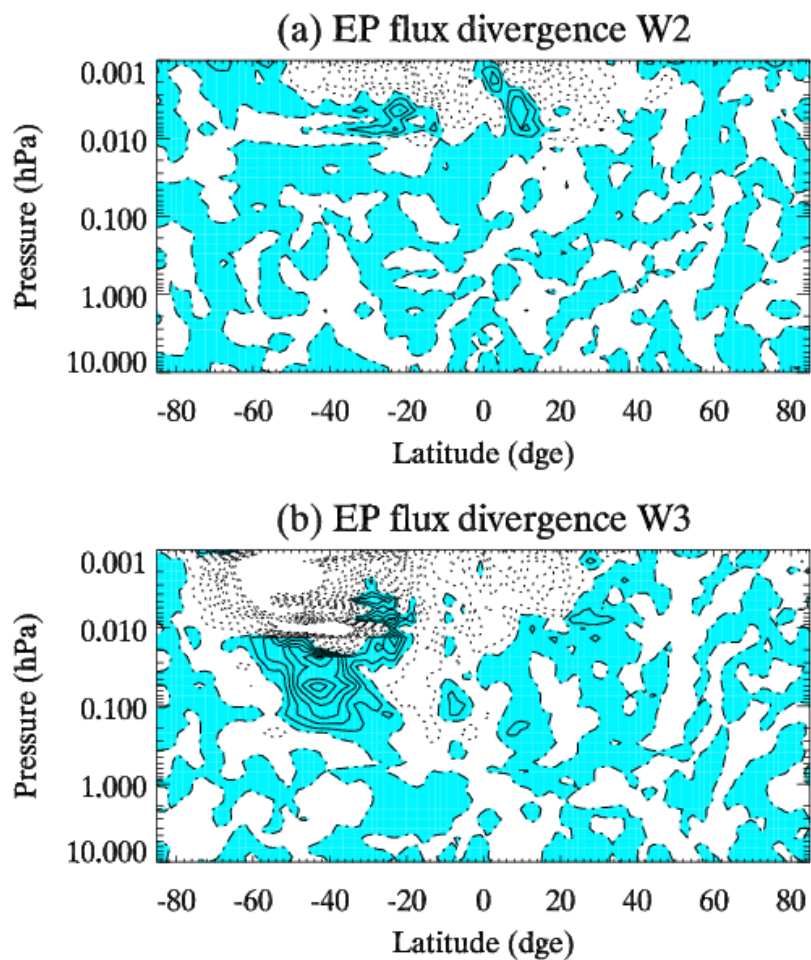
552



553

554 Figure 11 The same as Figure 10 but for the comparison between the critical lines of
555 the (red) 42-hour and (light green) 52-hour W3 QTDW during days 10-30 of 2006.

556



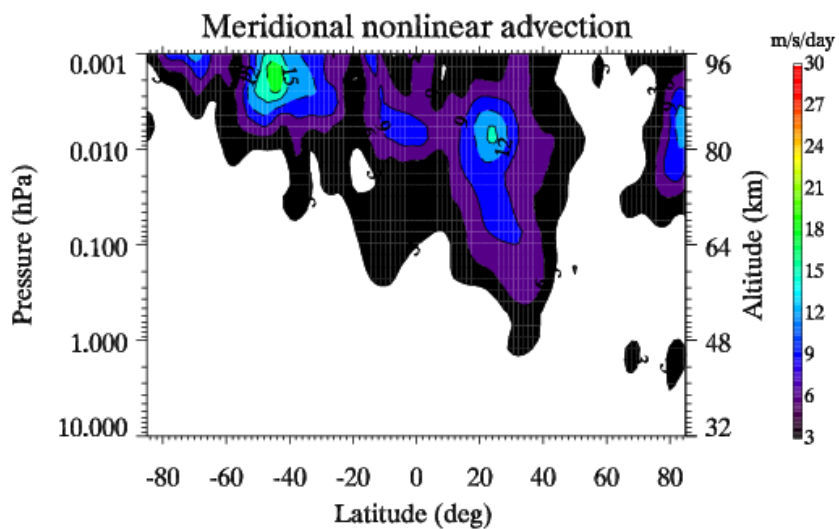
557

558 Figure 12 The EP flux divergence of (a) W2 and (b) W3 during January 23-30 of 2006.

559 The shaded region indicates positive EP flux divergence, and the contour interval is 2

560 m/s/day.

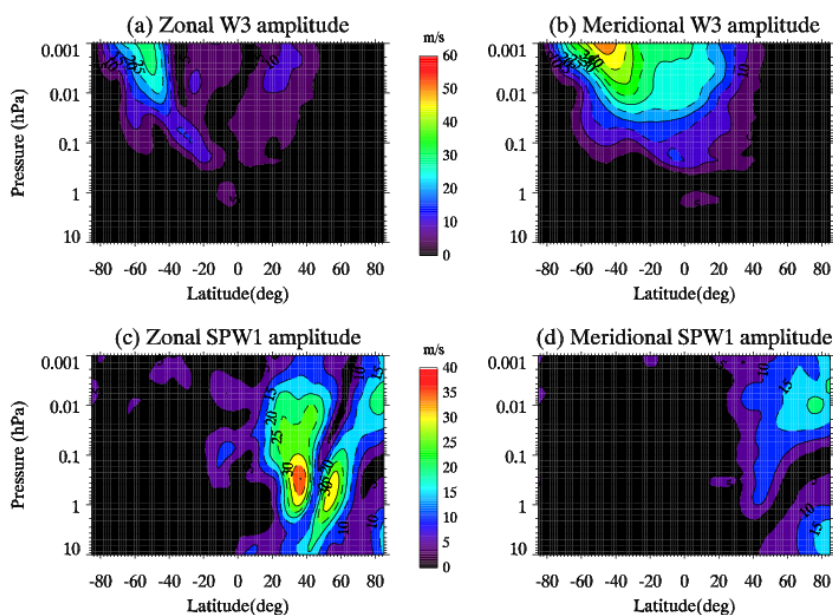
561



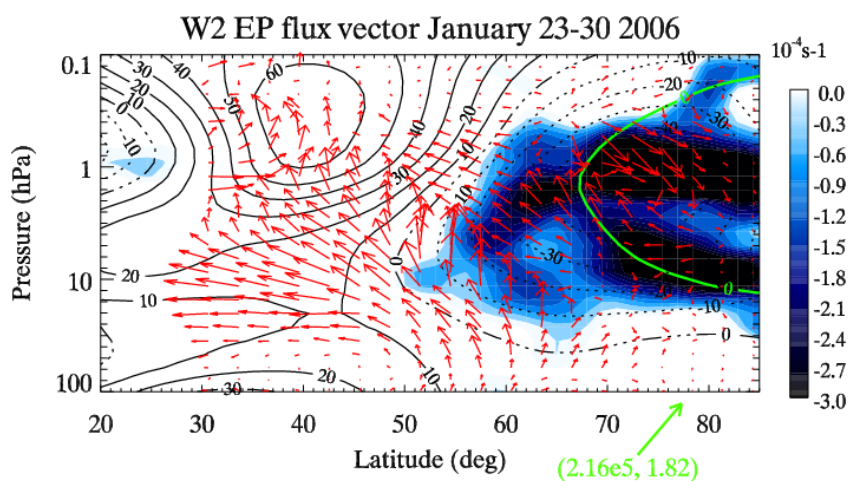
562

563 Figure 13 Meridional component of the nonlinear advection between W3 and SPW1
564 during January 23-30 of 2006.

565



566
 567 Figure 14. Altitude-latitude structures of (a, b) W3 and (c, d) SPW1 in (a, c) zonal and
 568 (b, d) meridional winds during January 23-30 of 2006.
 569



570
 571 Figure 15. The EP flux vectors of W2 and the mean flow instabilities during January
 572 23-30 near the winter stratosphere. The EP flux vectors are normalized by the square
 573 root of the neutral density. The reference length is shown at right bottom.